A Method for Calculating the Frequency-Dependent Properties of Microstrip Discontinuities

WOLFGANG MENZEL AND INGO WOLFF

Abstract—**A method is described for calculating the dynamical (frequency-dependent) properties of various microstrip discontinuities such as unsymmetrical crossings, T junctions, right-angle bends, impedance steps, and filter elements. The method is applied to an unsymmetrical T junction with three different linewidths. Using a waveguide model with frequency-dependent parameters, a field matching method proposed by Kühn is employed to compute the scattering matrix of the structures. The elements of the scattering matrix calculated in this way differ from those derived from static methods by a higher frequency dependence, especially for frequencies near the cutoff frequencies of the higher order modes on the microstrip lines. The theoretical results are compared with measurements, and theory and experiment are found to correspond closely.**

I. Introduction

MICROSTRIP discontinuities such as crossings, T junctions, bends, and impedance steps are elements of many complex microstrip circuits like filters, power dividers, ring couplers, and impedance transformers. Therefore, knowledge of the exact reflection and transmission properties in dependence on the frequency is of great importance. Various approaches have been made to calculate equivalent circuits for those discontinuities. Oliner [1] used Babinet's principle to describe stripline discontinuities, Silvester and Benedek [2]–[4], and Stouten [5] calculated the capacitances of microstrip discontinuities, and Gopinath and Silvester [6], Gopinath and Easter [7], and Thomson and Gopinath [8] computed the inductive elements of the equivalent circuits. All the methods described in these papers are based on static approximations, and therefore are valid with sufficient accuracy only for low frequencies.

A method is presented in this paper for calculating the transmission properties of the discontinuities, taking into account the frequency-dependent energy stored in higher order cutoff modes of the microstrip line. A waveguide model for the microstrip line, described in [9], [10], and a field matching technique proposed by Kühn [11] are used. This method has the advantage that complex microstrip circuits containing discontinuities can be calculated in a way similar to that shown by Rozzi and Mecklenbräuker [12] for waveguide circuits recently. Earlier papers, which used the waveguide model, only described less complex structures, as for example symmetrical T junctions [17].

As comparisons of the theoretical results and the measurements show, the dependence of the scattering matrix of microstrip discontinuities on the frequency is well approximated in a wide frequency range by the theory given in this paper.

Manuscript received January 29, 1976; revised May 2, 1976.
The authors are with the Department of Electrical Engineering, University of Duisburg, Duisburg, Germany.

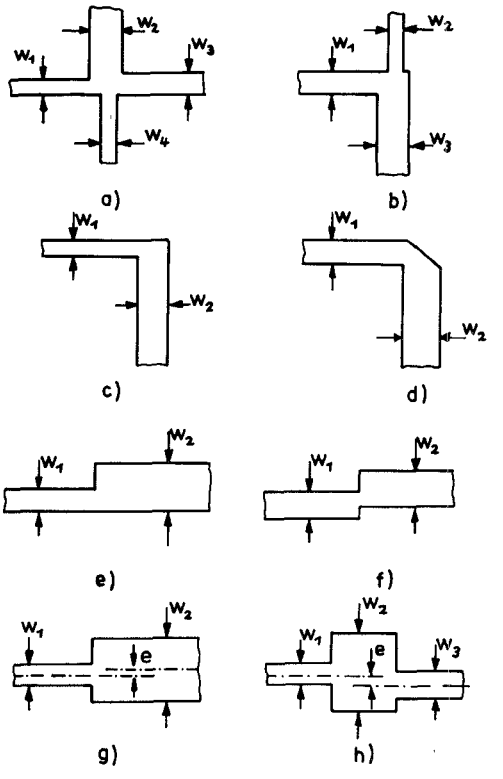

Fig. 1. Microstrip discontinuities which can be calculated by the theory described in this paper.

II. The Formulation of the Field Problem

It is the aim of this paper, to develop a field theoretical method for calculating the transmission properties of microstrip discontinuities, some of which are shown in Fig. 1.

For all discontinuities it is allowed that lines of different widths are connected to each other. In contrast to most of the theories described in previous papers, the method can be applied to unsymmetrical discontinuities. It is to be explained by the example of an unsymmetrical microstrip T junction (Fig. 3).

The dynamical properties of the microstrip lines are described using a waveguide model (Fig. 2). It consists of a parallel plate waveguide of width w_{eff} and height h with

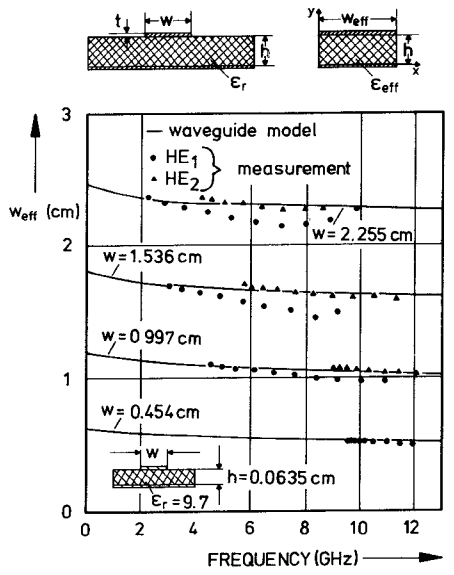

Fig. 2. Waveguide model of a microstrip line and effective width of the waveguide in dependence on the frequency. After [10].

plates of infinite conductivity at the top and bottom and with magnetic side walls. It is filled with a dielectric medium of the dielectric constant ε_{eff}. The effective width as well as the effective dielectric constant are frequency dependent. The height h of the waveguide model is equal to the height of the microstrip substrate material; ε_{eff} is the frequency-dependent effective dielectric constant as it can be computed for the microstrip line (e.g., [13]). The width of the waveguide model to a first approximation can be assumed to be equal to the frequency-independent effective width given by Wheeler [14]. As further investigations show [10], the effective width must also be frequency dependent. This is due to the physical fact that for higher frequencies the electromagnetic field is increasingly concentrated in the dielectric medium. The frequency-dependent effective width can be calculated from the characteristic impedance of the quasi-TEM mode (e.g., [15]), if the frequency-dependent effective dielectric constant is known. In Fig. 2 theoretical and experimental results for w_{eff} in dependence on the frequency are shown [10].

As in the case of the effective dielectric constant [16], a simple formula can be found to describe the frequency dependence of w_{eff} with sufficient accuracy in the relevant frequency range [17]

$$w_{\text{eff}}(f) = w + \frac{w_{\text{eff}}(0) - w}{1 + f/f_c} \tag{1}$$

where w is the width of the microstrip line, $w_{\text{eff}}(0)$ is the static value of the effective width according to Wheeler [14], and $f_c = c_0/(2w\varepsilon_r^{1/2})$, where ε_r is the dielectric constant of the substrate material.

It is assumed that the height h of the microstrip line and the waveguide model is so small that the fields of the waveguide model are independent of the y coordinate (Fig. 2) in the relevant frequency range. At the top and bottom the tangential electric field strength must vanish. So only a

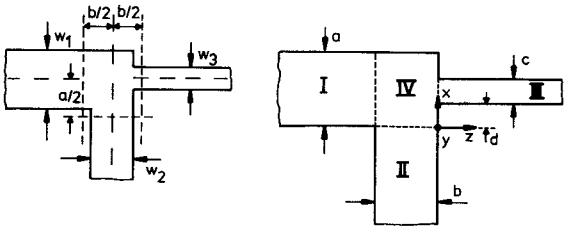

Fig. 3. Unsymmetrical microstrip T junction and introduced coordinate system.

TEM mode and TE_{n0} modes with E_y, H_x, and H_z components exist. The transversal electromagnetic field can be described using a scalar potential

$$\psi_{p0} = \sqrt{\frac{\varepsilon_p}{w_{\text{eff}}h}} \frac{\sin\left(\frac{p\pi}{w_{\text{eff}}}x\right)}{\frac{p\pi}{w_{\text{eff}}}}, \qquad \varepsilon_p = \begin{cases} 1 \text{ for } p = 0 \\ 2 \text{ for } p \neq 0 \end{cases} \tag{2}$$

by the equations

$$\begin{aligned} \boldsymbol{E}_t &= \sum_{p=0}^{\infty} (A_p e^{-\gamma z} + B_p e^{+\gamma z})(\boldsymbol{a}_z \times \nabla_t \psi_{p0}) \\ \boldsymbol{H}_t &= -\sum_{p=0}^{\infty} Y_{p0}(A_p e^{-\gamma z} - B_p e^{+\gamma z})\nabla_t \psi_{p0}. \end{aligned} \tag{3}$$

A_p and B_p are the amplitude coefficients, $\gamma = [(p\pi/w_{\text{eff}})^2 - \omega^2\varepsilon_{\text{eff}}\varepsilon_0\mu_0]^{1/2}$ is the propagation constant, $\boldsymbol{a}_z$ is the unit vector of the z coordinate, ∇_t is the transversal Nabla operator, and $Y_{p0} = 1/Z_{p0} = \gamma/(j\omega\mu_0)$ is the complex characteristic wave admittance. Using normalized wave amplitudes and introducing the potential function, the transversal components of the electric and magnetic fields are given by

$$\begin{aligned} E_y &= \sum_{p=0}^{\infty} (a_p e^{-\gamma z} + b_p e^{+\gamma z})\sqrt{Z_{p0}}\sqrt{\frac{\varepsilon_p}{w_{\text{eff}}h}}\cos\left(\frac{p\pi}{w_{\text{eff}}}x\right) \\ H_x &= -\sum_{p=0}^{\infty} (a_p e^{-\gamma z} - b_p e^{+\gamma z})\sqrt{Y_{p0}}\sqrt{\frac{\varepsilon_p}{w_{\text{eff}}h}}\cos\left(\frac{p\pi}{w_{\text{eff}}}x\right) \end{aligned} \tag{4}$$

where $a_p = Z_{p0}^{1/2} \cdot A_p$ and $b_p = Z_{p0}^{1/2} \cdot B_p$.

In Fig. 3 an unsymmetrical microstrip T junction and the equivalent waveguide circuit is shown. a, b, and c are the effective widths of the three microstrip lines. The waveguide T junction is divided into four regions. The regions I, II, and III are filled with a dielectric medium of effective dielectric constants $\varepsilon_{\text{eff}1}$, $\varepsilon_{\text{eff}2}$, and $\varepsilon_{\text{eff}3}$, corresponding to the three microstrip lines. In region IV an equivalent dielectric constant as defined in [18] for a microstrip disk capacitor is introduced, taking into account the electric stray field only at those sides of the region where no microstrip line is connected. The reference planes in the waveguide model are chosen to be the interfaces between region IV and the regions I, II, and III. Accordingly, the reference planes of the microstrip T junction are defined as shown in Fig. 3.

A complete solution for the electromagnetic field in the regions I, II, and III can be given by analogy with (4) taking into consideration the change of the coordinates:

$$E_y^{\mathrm{I}} = \sum_{p=0}^{\infty} \sqrt{Z_p^{\mathrm{I}}}(a_p^{\mathrm{I}} e^{-\gamma(z+b)} + b_p^{\mathrm{I}} e^{+\gamma(z+b)}) \cdot \sqrt{\frac{\varepsilon_p}{ah}} \cos\left(\frac{p\pi}{a} x\right)$$

$$H_x^{\mathrm{I}} = -\sum_{p=0}^{\infty} \sqrt{Y_p^{\mathrm{I}}}(a_p^{\mathrm{I}} e^{-\gamma(z+b)} - b_p^{\mathrm{I}} e^{+\gamma(z+b)}) \cdot \sqrt{\frac{\varepsilon_p}{ah}} \cos\left(\frac{p\pi}{a} x\right) \tag{5a}$$

$$E_y^{\mathrm{II}} = \sum_{k=0}^{\infty} \sqrt{Z_k^{\mathrm{II}}}(a_k^{\mathrm{II}} e^{-\gamma x} - b_k^{\mathrm{II}} e^{+\gamma x}) \sqrt{\frac{\varepsilon_k}{bh}} \cos\left(\frac{k\pi}{b} z\right)$$

$$H_z^{\mathrm{II}} = \sum_{k=0}^{\infty} \sqrt{Y_k^{\mathrm{II}}}(a_k^{\mathrm{II}} e^{-\gamma x} - b_k^{\mathrm{II}} e^{+\gamma x}) \sqrt{\frac{\varepsilon_k}{bh}} \cos\left(\frac{k\pi}{b} z\right) \tag{5b}$$

$$E_y^{\mathrm{III}} = \sum_{m=0}^{\infty} \sqrt{Z_m^{\mathrm{III}}}(a_m^{\mathrm{III}} e^{+\gamma z} + b_m^{\mathrm{III}} e^{-\gamma z}) \cdot \sqrt{\frac{\varepsilon_m}{ch}} \cos\left(\frac{m\pi}{c}(x-d)\right)$$

$$H_x^{\mathrm{III}} = \sum_{m=0}^{\infty} \sqrt{Y_m^{\mathrm{III}}}(a_m^{\mathrm{III}} e^{+\gamma z} - b_m^{\mathrm{III}} e^{-\gamma z}) \cdot \sqrt{\frac{\varepsilon_m}{ch}} \cos\left(\frac{m\pi}{c}(x-d)\right). \tag{5c}$$

Following Kühn [11], the field in region IV is found by superimposing three standing wave solutions:

$$E_y^{\mathrm{IV}a} = \sum_{p=0}^{\infty} \sqrt{\bar{Z}_p^{\mathrm{I}}}\, c_p^{\mathrm{IV}a} \cos(\bar{\beta}^{\mathrm{I}} z) \cos\left(\frac{p\pi}{a} x\right) \sqrt{\frac{\varepsilon_p}{ah}}$$

$$H_x^{\mathrm{IV}a} = j \sum_{p=0}^{\infty} \sqrt{\bar{Y}_p^{\mathrm{I}}}\, c_p^{\mathrm{IV}a} \sin(\bar{\beta}^{\mathrm{I}} z) \cos\left(\frac{p\pi}{a} x\right) \sqrt{\frac{\varepsilon_p}{ah}} \tag{6a}$$

$$E_y^{\mathrm{IV}b} = \sum_{k=0}^{\infty} \sqrt{\bar{Z}_k^{\mathrm{II}}}\, c_k^{\mathrm{IV}b} \cos(\bar{\beta}^{\mathrm{II}}(x-a)) \cos\left(\frac{k\pi}{b} z\right) \sqrt{\frac{\varepsilon_k}{bh}}$$

$$H_z^{\mathrm{IV}b} = -j \sum_{k=0}^{\infty} \sqrt{\bar{Y}_k^{\mathrm{II}}}\, c_k^{\mathrm{IV}b} \sin(\bar{\beta}^{\mathrm{II}}(x-a)) \cos\left(\frac{k\pi}{b} z\right) \cdot \sqrt{\frac{\varepsilon_k}{bh}} \tag{6b}$$

$$E_y^{\mathrm{IV}c} = \sum_{m=0}^{\infty} \sqrt{\bar{Z}_m^{\mathrm{I}}}\, c_m^{\mathrm{IV}c} \cos(\bar{\beta}^{\mathrm{I}}(z+b)) \cos\left(\frac{m\pi}{a} x\right) \sqrt{\frac{\varepsilon_m}{ah}}$$

$$H_x^{\mathrm{IV}c} = j \sum_{m=0}^{\infty} \sqrt{\bar{Y}_m^{\mathrm{I}}}\, c_m^{\mathrm{IV}c} \sin(\bar{\beta}^{\mathrm{I}}(z+b)) \cos\left(\frac{m\pi}{a} x\right) \sqrt{\frac{\varepsilon_m}{ah}}. \tag{6c}$$

$\bar{\beta}^{\nu}$ (ν = I,II) are the phase constants of region I or II, respectively, calculated with the equivalent dielectric constant of region IV instead of $\varepsilon_{\mathrm{eff}1}$ or $\varepsilon_{\mathrm{eff}2}$. In the same way $\bar{Z}_{\nu}^{\mu}$ is calculated from Z_{ν}^{μ}.

Matching the magnetic field strength of regions I, II, and III to that of region IV, in each case only one term of the superimposed field after (6) must be taken into account, because of the boundary conditions of the magnetic walls. The connections between the field amplitudes of regions I and IV, and II and IV, can be found simply by comparison of the coefficients

$$c_p^{\mathrm{IV}a} = -j \frac{a_p^{\mathrm{I}} - b_p^{\mathrm{I}}}{\sin(\bar{\beta}_p^{\mathrm{I}} b)} \sqrt{\frac{\bar{Z}_p^{\mathrm{I}}}{Z_p^{\mathrm{I}}}} \tag{7}$$

and

$$c_k^{\mathrm{IV}b} = -j \frac{a_k^{\mathrm{II}} - b_k^{\mathrm{II}}}{\sin(\bar{\beta}_k^{\mathrm{II}} a)} \sqrt{\frac{\bar{Z}_k^{\mathrm{II}}}{Z_k^{\mathrm{II}}}} \tag{8}$$

whereas the coefficients of regions III and IV must be determined by a normal mode matching procedure at the interface III–IV:

$$c_M^{\mathrm{IV}c} = -j \sum_{m=0}^{\infty} \sqrt{\frac{\bar{Z}_M^{\mathrm{I}}}{Z_m^{\mathrm{III}}}} \frac{a_m^{\mathrm{III}} - b_m^{\mathrm{III}}}{\sin(\bar{\beta}_M^{\mathrm{I}} b)} \cdot K_{[m,M]}^{(1)} \tag{9}$$

with

$$K_{[m,M]}^{(1)} = \frac{\sqrt{\varepsilon_m \varepsilon_M}}{\sqrt{ac} \cdot h} \int_{z=0}^{} \int \cos\left(\frac{m\pi}{c} x\right) \cos\left(\frac{M\pi}{a} x\right) dx\, dy.$$

If the electric field strength of regions I, II, and III is to be matched to the electric field of region IV, the tangential components of all three standing wave solutions [see (6)] have to be taken into account. This will be shown by the example of the field matching between regions I and IV. The tangential electric field of region IV in the plane $z = -b$ [Fig. 3(b)] is given by

$$E_y^{\mathrm{IV}}|_{z=-b} = E_y^{\mathrm{IV}a}|_{z=-b} + E_y^{\mathrm{IV}b}|_{z=-b} + E_y^{\mathrm{IV}c}|_{z=-b}. \tag{10}$$

Matching this field to that of region I leads to an equation which connects the amplitude coefficients of regions I and IV:

$$\sqrt{Z_P^{\mathrm{I}}}(a_P^{\mathrm{I}} + b_P^{\mathrm{I}}) = \sqrt{\bar{Z}_P^{\mathrm{I}}}\, c^{\mathrm{IV}a} \cos(\bar{\beta}_P^{\mathrm{I}} b) + \sqrt{\bar{Z}_P^{\mathrm{I}}}\, c_P^{\mathrm{IV}c} + \sum_{k=0}^{\infty} \sqrt{\bar{Z}_k^{\mathrm{II}}}\, c_k^{\mathrm{IV}b} K_{[k,P]}^{(2)} \tag{11}$$

with

$$K_{[k,P]}^{(2)} = (-1)^P \int_{z=-b}^{} \int \sqrt{\frac{\varepsilon_k \varepsilon_P}{ba}} \frac{1}{h} \cdot \cos(\bar{\beta}_k^{\mathrm{II}}(x-a)) \cos\left(\frac{P\pi}{a} x\right) dx\, dy.$$

In the same way the electric fields of regions II and III are matched to that of region IV.

From (7)–(9) the coefficients $c_{\nu}^{\mathrm{IV}a}$, $c_{\nu}^{\mathrm{IV}b}$, and $c_{\nu}^{\mathrm{IV}c}$ can be eliminated and introduced into the matching conditions of the electric field strength. In this way a set of $P + K + M + 3$ equations results, which connects the amplitudes a_{ν}^{I}, a_{μ}^{II}, a_{η}^{III} ($\nu,\mu,\eta = 0,1,2,\cdots$) of the incident waves to the coefficients b_{ν}^{I}, b_{μ}^{II}, b_{η}^{III} of the reflected or transmitted waves.

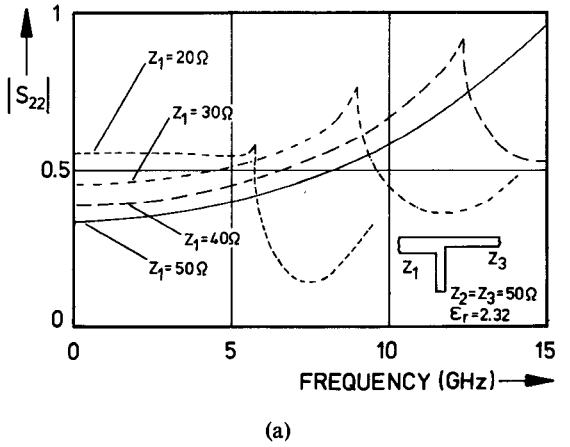

Fig. 4. Reflection coefficient $|S_{22}|$ (a) and transmission coefficient $|S_{23}|$ (b) of an unsymmetrical T junction with $Z_2 = Z_3 = 50\,\Omega$ and different values of Z_1. Substrate material Polyguide: $\varepsilon_r = 2.32$, $h = 0.158$ cm.

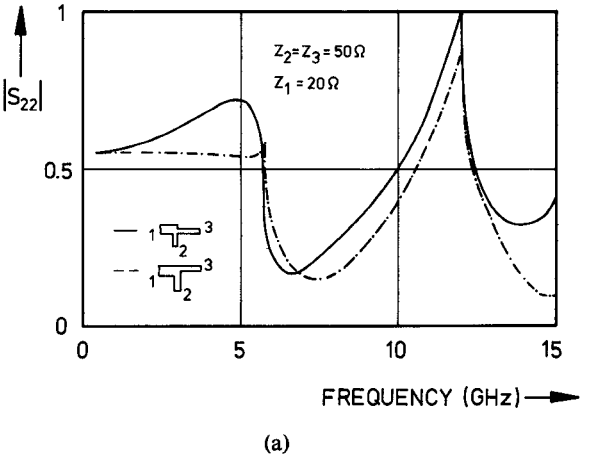

Fig. 5. Reflection coefficient $|S_{22}|$ (a) and transmission coefficient $|S_{23}|$ (b) for two T junctions of equal characteristic impedances but different geometrical structure. Substrate material Polyguide: $\varepsilon_r = 2.32$, $h = 0.158$ cm.

P,K,M are the numbers of the highest order modes which are taken into account if the equations are evaluated numerically. If only an incident TEM mode at one port of the T junction is considered, the scattering parameters can easily be computed from the amplitudes of the incident and reflected or transmitted waves.

III. Numerical Results

The resulting equations have been evaluated numerically for different unsymmetrical microstrip T junctions on Polyguide substrate material. No relative convergence problems occur, and the results are of sufficient accuracy (error < 0.5 percent) even if only five higher order modes are taken into account in each line and the connecting field region.

The results shown in Figs. 4–6 have been computed with eight higher order modes. In this case a computing time (central processing time on a CD Cyber 72/76) of 50 ms is required for the calculation of the scattering matrix at one frequency. Fig. 4 shows the reflection coefficients $|S_{22}|$ and the transmission coefficients $|S_{23}|$ of T junctions with the characteristic impedances $Z_2 = Z_3 = 50\ \Omega$ and different values of Z_1 on Polyguide material. At low frequencies ($f < 2$ GHz) the coefficients can be calculated from the static characteristic impedances. For higher frequencies the coefficients become frequency dependent. The reflection coefficients increase with increasing frequency, until they

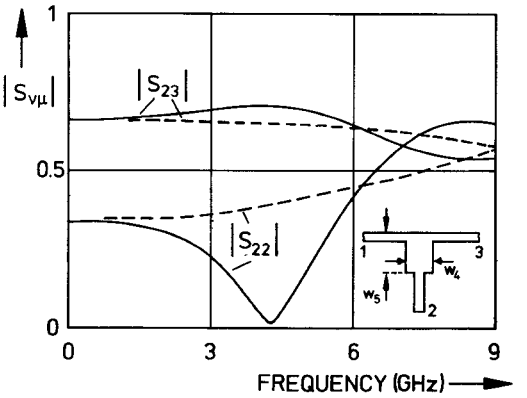

Fig. 6. Elements of the scattering matrix of a compensated microstrip T junction. ——— compensated T junction. ------ uncompensated T junction. $Z_1 = Z_2 = Z_3 = 50\ \Omega$. $w_4 = 1$ cm, $w_5 = 2$ cm. Substrate material Polyguide: $\varepsilon_r = 2.32$, $h = 0.158$ cm.

reach a maximum at the cutoff frequency of the first higher order mode. The transmission coefficients decrease with increasing frequency. If $Z_1 = Z_3$, the maximum value of $|S_{22}|$ becomes 1, whereas $|S_{23}|$ decreases to zero. For different impedances of line 1 and line 2 the maximum value of $|S_{22}|$ decreases with increasing difference between the impedances. For frequencies higher than the cutoff frequency of the first higher order mode (normally this frequency range is not of great interest for practical use),

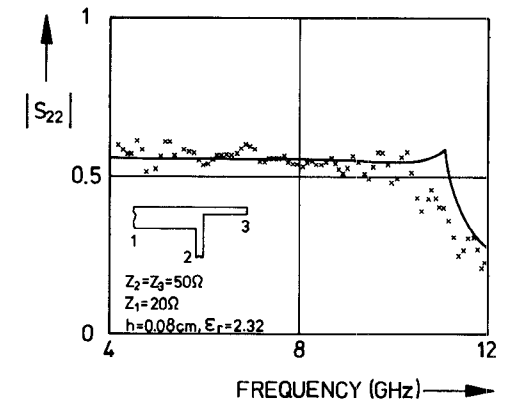

(a)

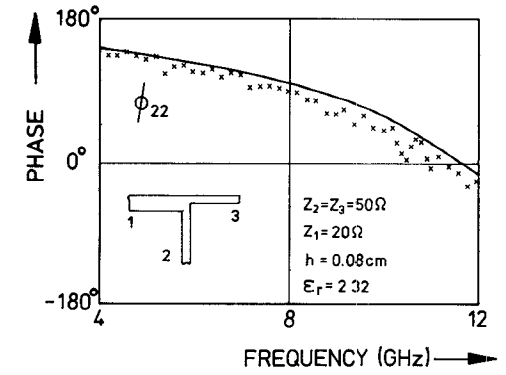

(b)

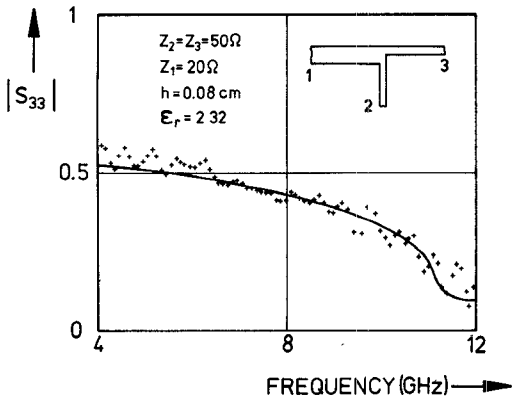

(c)

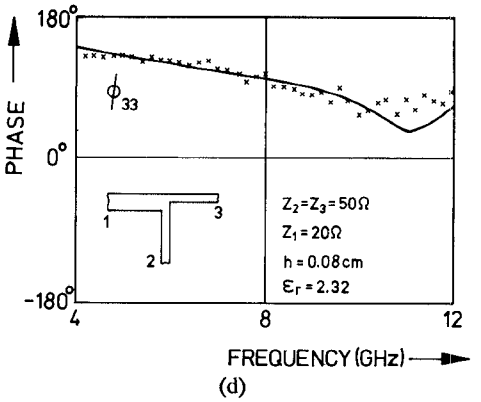

(d)

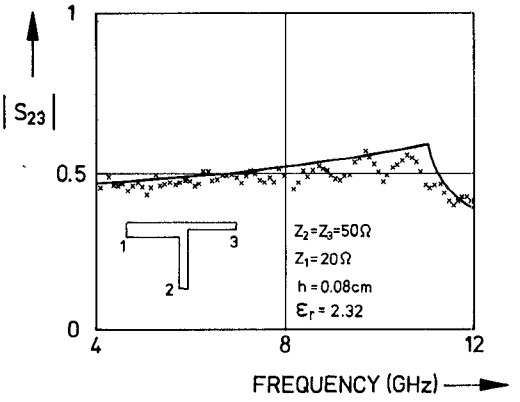

(e)

Fig. 7. Measured and calculated scattering parameters of an unsymmetrical T junction on Polyguide material.

the reflection coefficients strongly decrease and again have a second maximum at the next cutoff frequency. For a 0.158-cm-thick Polyguide substrate material, which has a small dielectric constant, the variation of the reflection coefficient $|S_{22}|$ from 0 to 10 GHz is about 100 percent. The frequency dependence of the scattering matrix becomes smaller with decreasing values of height h and increasing dielectric constant ε_r, if the same frequency range is considered.

The calculation method described can also be used to study the influence of the geometrical structure on the transmission properties of discontinuities. By way of an example, Fig. 5 shows the reflection coefficients $|S_{22}|$ and the transmission coefficients $|S_{23}|$ for two unsymmetrical T junctions with equal characteristic impedances but different geometrical structures. It can clearly be recognized that a stronger frequency dependence arises if the discontinuity contains additional edges.

This result can be used, for example, to design compensated microstrip power dividers. As is shown in Fig. 6, the reflection coefficient $|S_{22}|$ of a T junction can be made zero at one frequency, if the widths w_1 and w_2 of the first and second microstrip line are smaller than the widths of the connecting field region. This T junction can be calculated in a similar manner to that described previously. As Fig. 6 shows, the reflection coefficient $|S_{22}|$ over a frequency range of 6 GHz is smaller than that of the uncompensated T junction with the same characteristic impedances.

IV. Experimental Results

Measurements have been performed with T junctions on Polyguide material ($\varepsilon_r = 2.32$, $h = 0.0794$ cm) and have been compared to theoretical results. The measurements were carried out on an HP network analyzer connected to an automatic data acquisition system. An attempt was made to eliminate the influence of the microstrip-coax transitions on the measurements by determining the reflection and transmission coefficients of the transitions and correcting the measured scattering parameters. Because of difficulties with the terminations, deviations larger than the inaccuracies of the network analyzer occur. The influence of the line losses on the results have been taken into consideration, whereas radiation losses, which occur especially for substrate materials of small dielectric constant and large height, could not be taken into account.

Figs. 7 and 8 show the measured and computed scattering parameters of two T junctions with 20–50–50 Ω and 50–

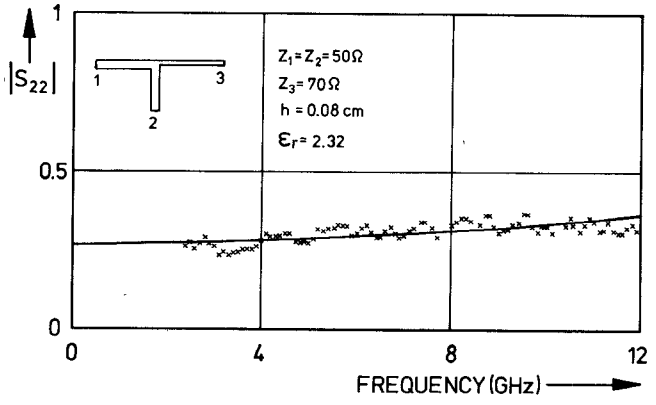

(a)

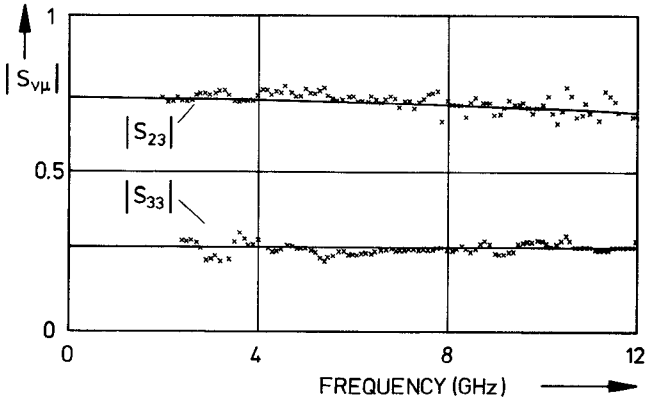

(b)

Fig. 8. Measured and calculated scattering parameters of an unsymmetrical T junction on Polyguide material.

50–70 Ω impedances as examples. All the measured absolute values and phases, in the light of the remarks made previously, correspond closely to theoretical results. Larger deviations between theory and experiment occur for thicker substrates, especially near the cutoff frequencies, for at these frequencies the radiated power becomes large. Additional difficulties occur with the measurements of those discontinuities, for the termination of lines of larger width is much more complicated. For example, Fig. 9 shows the calculated and measured results for a T junction on Polyguide material of height $h = 0.158$ cm. At low frequencies the termination of the 40-Ω line is very difficult, giving rise to the deviations between theory and experiment at 4 GHz. For frequencies near the cutoff frequency ($f \approx 12$ GHz) the measured reflection coefficient is smaller than the calculated one because of the radiated power.

V. Conclusions

A method is presented which can be used to calculate the dynamical properties of many microstrip discontinuities. As far as the authors know, this is the first method described in the literature for calculating the frequency-dependent properties of unsymmetrical microstrip discontinuities. In the case of normally used frequency ranges and microstrip lines, the method leads to results which are strongly supported by measurements. The computer

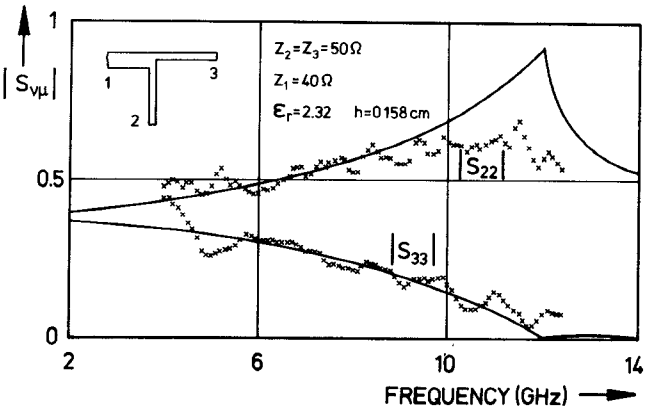

Fig. 9. Measured and calculated scattering parameters of an unsymmetrical T junction on thick Polyguide material.

programs do not need much computer storage and are relatively fast, so they can also be used in computer-aided design methods. Further developments of the existing programs may lead to the possibility of studying compensation methods for power dividers or similar circuits.

References

[1] A. A. Oliner, "Equivalent circuits for discontinuities in balanced strip transmission line," *IEEE Trans. Microwave Theory Tech. (Special Issue on Symp. on Microwave Strip Circuits)*, vol. MTT-3, pp. 134–143, Nov. 1955.
[2] P. Silvester and P. Benedek, "Equivalent capacitances of microstrip open circuits," *IEEE Trans. Microwave Theory Tech.*, vol. MTT-20, pp. 511–516, Aug. 1972.
[3] P. Benedek and P. Silvester, "Equivalent capacitances of microstrip gaps and steps," *IEEE Trans. Microwave Theory Tech.*, vol. MTT-20, pp. 729–733, Nov. 1972.
[4] P. Silvester and P. Benedek, "Microstrip discontinuity capacitances for right-angle bends, T-junctions and crossings," *IEEE Trans. Microwave Theory Tech.*, vol. MTT-21, pp. 341–346, May 1973.
[5] P. Stouten, "Equivalent capacitances of T-junctions," *Electron. Lett.*, vol. 9, pp. 552–553, Nov. 1973.
[6] A. Gopinath and P. Silvester, "Calculation of inductance of finite-length strips and its variation with frequency," *IEEE Trans. Microwave Theory Tech.*, vol. MTT-21, pp. 380–386, June 1973.
[7] A. Gopinath and B. Easter, "Moment method of calculating discontinuity inductance of microstrip right angled bends," *IEEE Trans. Microwave Theory Tech.* (Short Papers), vol. MTT-22, pp. 880–883, Oct. 1974.
[8] A. Thompson and A. Gopinath, "Calculation of microstrip discontinuity inductance," *IEEE Trans. Microwave Theory Tech.*, vol. MTT-23, pp. 648–655, Aug. 1975.
[9] I. Wolff, G. Kompa, and R. Mehran, "Calculation method for microstrip discontinuities and T-junctions," *Electron. Lett.*, vol. 8, p. 177, Apr. 1972.
[10] G. Kompa and R. Mehran, "Planar waveguide model for calculating microstrip components," *Electron. Lett.*, vol. 11, pp. 459–460, Sept. 1975.
[11] E. Kühn, "A mode-matching method for solving field problems in waveguide and resonator circuits," *Arch. Elek. Übertragung*, vol. 27, pp. 511–513, Dec. 1973.
[12] T. E. Rozzi and W. F. G. Mecklenbräuker, "Wide-band network modeling of interacting inductive irises and steps," *IEEE Trans. Microwave Theory Tech.*, vol. MTT-23, pp. 235–245, Feb. 1975.
[13] R. Jansen, "A moment method for covered microstrip dispersion," *Arch. Elek. Übertragung*, vol. 29, pp. 17–20, 1975.
[14] H. A. Wheeler, "Transmission-line properties of parallel wide strips by a conformal-mapping approximation," *IEEE Trans. Microwave Theory Tech.*, vol. MTT-12, pp. 280–289, 1964.
[15] H. J. Schmitt and K. H. Sarges, "Wave propagation in microstrip," *Nachrichtentech. Z.*, vol. 24, pp. 260–264, 1971.
[16] M. V. Schneider, "Microstrip dispersion," *Proc. Inst. Elect. Electron. Engrs.*, vol. 60, pp. 144–146, 1972.
[17] R. Mehran, "The frequency-dependent scattering matrix of microstrip right-angle bends, T-junctions and crossings," *Arch. Elek. Übertragung*, vol. 29, pp. 454–460, Nov. 1975.
[18] I. Wolff, "Statische Kapazitäten von rechteckigen und kreisförmigen Mikrostrip-Scheibenkondensatoren," *Arch. Elek. Übertragung*, vol. 27, pp. 44–47, Jan. 1973.